J|A|C|S ARTICLES

Published on Web 05/28/2009

Functionalized Dendritic Oligothiophenes: Ruthenium Phthalocyanine Complexes and Their Application in Bulk Heterojunction Solar Cells

Markus K. R. Fischer,[†] Ismael López-Duarte,[‡] Martijn M. Wienk,[§] M. Victoria Martínez-Díaz,[‡] René A. J. Janssen,*[,§] Peter Bäuerle,*[,†] and Tomás Torres*[,‡]

Institute of Organic Chemistry II and Advanced Materials, University of Ulm, Albert-Einstein-Allee 11, D-89081 Ulm, Germany, Departamento de Química Orgánica, Universidad Autónoma de Madrid, E-28049 Cantoblanco, Spain, and Molecular Materials and Nanosystems, Eindhoven University of Technology, P.O. Box 513, NL-5600 MB Eindhoven, Netherlands

Received March 16, 2009; E-mail: peter.baeuerle@uni-ulm.de; tomas.torres@uam.es

Abstract: Within the present work, two series of novel ruthenium(II) phthalocyanine (RuPc) complexes with one [RuPcCOPy-*n*T] or two [RuPc(Py-*n*T)$_2$] dendritic oligothiophene (DOT) ligands in the axial positions are reported. The ability of Ru^{II} for axial coordination in RuPcs allowed the attachment of the Pc through the metal site to the DOT-ligands bearing pyridine at the core position of the dendrons. These extended pyridine functionalized conjugated DOT-ligands (Py-*n*T) were chosen to cover the spectral window between 380 and 550 nm, where the RuPc does not exhibit a strong absorption, in order to improve the light-absorption of these complexes and hence enhance the efficiency of the corresponding solar cells. Good efficiencies of up to 1.6% have been achieved when blended together with a fullerene acceptor in solution-processed photovoltaic devices, providing by far the best phthalocyanine-based bulk heterojunction solar cells reported to-date.

Introduction

Functional oligothiophenes have attracted comprehensive interest among researchers and actually been advanced to the most frequently used π-conjugated materials, in particular, as active components in organic electronic devices and molecular electronics such as solar cells.[1,2] Their unique electronic, optical, and redox properties are intriguing, as well as their unique self-assembling properties on solid surfaces or in the bulk.[3] Moreover, the high polarizability of sulfur atoms in thiophene rings leads to a stabilization of the conjugated chain in various redox states and to excellent charge transport properties which are one of the most crucial assets for applications in organic electronics. In this respect, different functionalized oligothiophenes were successfully implemented as donor and C_{60} as acceptor in vapor-deposited thin-film photovoltaic cells reaching high efficiencies of up to 3.4%.[4−6]

Dendritic oligothiophenes (DOTs) with a three-dimensional structure were first synthesized by Advincula et al. and were found to have interesting absorption properties and a conjugation gradient that is able to funnel the light energy.[7,8]

Over the past decade phthalocyanines[9] (Pc) have also emerged as a promising molecular component for artificial photosynthetic systems, since they exhibit large absorption in the visible region, contain large, conjugated π-systems suitable for efficient electron-transfer processes, and possess strongly reducing or oxidizing characteristics determined by the nature of the central metals and the peripheral substituents. In this context, we have designed and studied several series of either covalently linked[10,11] or supramolecularly assembled[12,13] phthalocyanine-based conjugates. Some of the aforementioned structures exhibited promising performances as constituents of photovoltaic devices.[14,15]

[†] University of Ulm.
[‡] Universidad Autónoma de Madrid.
[§] Eindhoven University of Technology.

(1) *Handbook of Oligo- and Polythiophenes*; Fichou, D., Ed.; Wiley-VCH: Weinheim, 1999.
(2) *Organic Electronics*; Klauk, H., Ed.; Wiley-VCH: Weinheim, 2006.
(3) Bäuerle, P. In *Electronic Materials: The Oligomer Approach*; Müllen, K., Wegner, G., Eds.; Wiley-VCH: Weinheim, 1998.
(4) Schulze, K.; Uhrich, C.; Schüppel, R.; Leo, K.; Pfeiffer, M.; Brier, E.; Reinold, E.; Bäuerle, P. *Adv. Mater.* **2006**, *18*, 2872.
(5) Uhrich, C.; Schueppel, R.; Petrich, A.; Pfeiffer, M.; Leo, K.; Brier, E.; Kilickiran, P.; Bäuerle, P. *Adv. Funct. Mater.* **2007**, *17*, 2991.
(6) Schulze, K.; Riede, M.; Brier, E.; Reinhold, E.; Bäuerle, P.; Leo, K. *J. Appl. Phys.* **2008**, *104*, 074511.
(7) Xia, C.; Fan, X.; Locklin, J.; Advincula, R. C. *Org. Lett.* **2002**, *4*, 2067.
(8) Xu, M.-H.; Pu, L. *Tetrahedron Lett.* **2002**, *43*, 6347.
(9) de la Torre, G.; Claessens, C. G.; Torres, T. *Chem. Commun.* **2007**, 2000.
(10) Campidelli, S.; Ballesteros, B.; Filoramo, A.; Díaz Díaz, D.; de la Torre, G.; Torres, T.; Rahman, G. M. A.; Ehli, C.; Kiessling, D.; Werner, F.; Sgobba, V.; Guldi, D. M.; Cioffi, C.; Prato, M.; Bourgoin, J.-P. *J. Am. Chem. Soc.* **2008**, *130*, 11503.
(11) Bottari, G.; Olea, D.; Gómez-Navarro, C.; Zamora, F.; Gómez-Herrero, J.; Torres, T. *Angew. Chem., Int. Ed.* **2008**, *47*, 2026.
(12) Ballesteros, B.; de la Torre, G.; Torres, T.; Hug, G. L.; Rahman, G. M. A.; Guldi, D. M. *Tetrahedron* **2006**, *62*, 2097.
(13) de la Escosura, A.; Martinez-Diaz, M. V.; Guldi, D. M.; Torres, T. *J. Am. Chem. Soc.* **2006**, *128*, 4112.

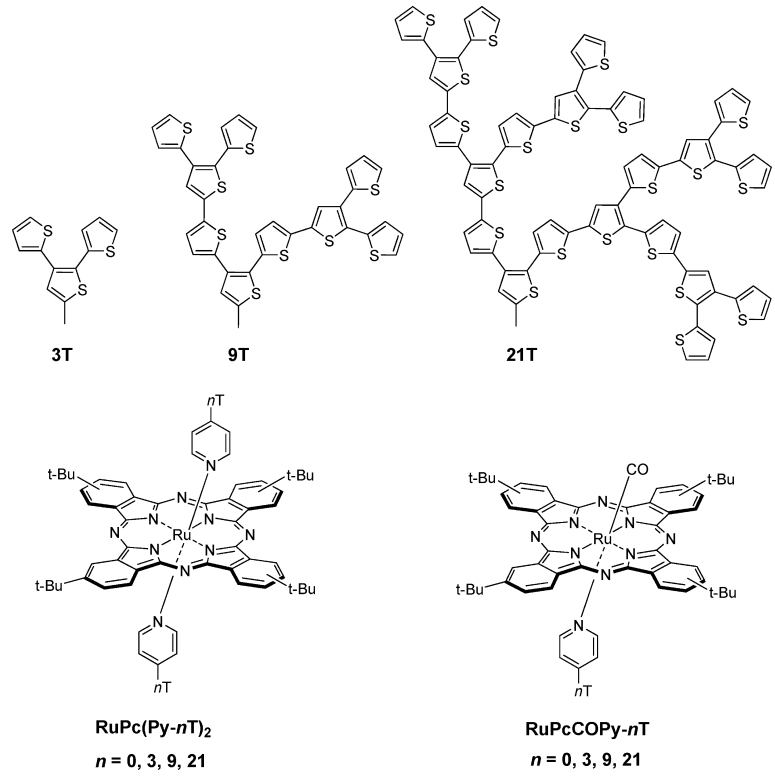

Figure 1. Molecular structures of the RuPcCOPy-*n*T or RuPc(Py-*n*T)$_2$ complexes (n = 0, 3, 9, 21).

Unsubstituted phthalocyanines are typically poorly soluble in common organic solvents, enforcing application of vapor deposition techniques for their incorporation into solar cells. Solar cells consisting of CuPc as donor and C_{60} as acceptor are among the most intensively investigated, reaching high efficiencies of up to 5% with highly advanced device architectures.[16] Other metallo-Pcs (such as ZnPc or SnPc) have been blended with different acceptors for photovoltaic applications with limited success.[17−20] Only one publication described the incorporation of RuPc into heterojunction solar cells.[21] These cells have been prepared by vapor deposition, and no efficiencies were stated. Very low EQE-maxima of less than 0.18% were given and point to the assumption that the cells were almost ineffective. Solution processed phthalocyanine-based bulk heterojunction solar cells (BHJSC) are very rarely reported.[22−24] Efficiencies of up to 0.08% were reported for devices using soluble discotic liquid crystalline CuPcs and C_{60} in a partially solution-processed solar cell.[22]

By virtue of all these results we decided to synthesize soluble phthalocyanine complexes which can be applied in solution processed BHJSCs to bridge the gap between the highly efficient phthalocyanine solar cells prepared by vapor deposition technique and the almost ineffective solution processed counterparts to some extent. Therefore, we used phthalocyanines with four solubilizing peripheral *t*Bu groups that incorporated ruthenium as metal center. This metal allows the introduction of two additional axial ligands next to the phthalocyanine, which additionally avoid macrocycle aggregation. We intended to use π-conjugated ligands as the axial ligands which help to enhance the light-harvesting ability of the complex and are not detrimental to the solubility of the whole system. As some of us already introduced well soluble dendritic oligothiophenes as a new class of highly soluble 3D-macromolecular semiconductors which showed good performance in BHJSCs,[25,26] we decided to merge these systems with the soluble RuPc complex. Pyridine units have been introduced in the core position of the dendritic oligothiophenes (DOTs) as complexation site to result in pyridine-functionalized dendritic oligothiophenes (Py-*n*T).[26] These ligands have been synthesized up to the third generation (G3), bearing an increasing number of conjugated thiophene units with increasing generation. The resulting ruthenium

(14) O'Regan, B. C.; Lopez-Duarte, I.; Martinez-Diaz, M. V.; Forneli, A.; Albero, J.; Morandeira, A.; Palomares, E.; Torres, T.; Durrant, J. R. *J. Am. Chem. Soc.* **2008**, *130*, 2906.
(15) Cid, J.-J.; Yum, J.-H.; Jang, S.-R.; Nazeeruddin, M. K.; Palomares, E.; Ko, J.; Grätzel, M.; Torres, T. *Angew. Chem., Int. Ed.* **2007**, *46*, 8358.
(16) Xue, J.; Rand, B. P.; Uchida, S.; Forrest, S. R. *Adv. Mater.* **2005**, *17*, 66.
(17) Koeppe, R.; Bossart, O.; Calzaferri, G.; Sariciftci, N. S. *Sol. Energy Mater. Sol. Cells* **2007**, *91*, 986.
(18) Bernède, J. C.; Derouiche, H.; Djara, V. *Sol. Energy Mater. Sol. Cells* **2005**, *87*, 261.
(19) Gebeyehu, D.; Maennig, B.; Drechsel, J.; Leo, K.; Pfeiffer, M. *Sol. Energy Mater. Sol. Cells* **2003**, *79*, 81.
(20) Sharma, G. D.; BalaRaju, P.; Roy, R. S. *Sol. Energy Mater. Sol. Cells* **2008**, *92*, 261.
(21) Capobianchi, A.; Tucci, M. *Thin Solid Films* **2004**, *451−452*, 33.
(22) Yoo, S.; Domercq, B.; Donley, C. L.; Carter, C.; Xia, W.; Minch, B. A.; O'Brien, D. F.; Armstrong, N. R.; Kippelen, B. In *Organic Photovoltaics IV*, 1st ed.; SPIE: San Diego, CA, 2004; Vol. 5215, p 71.
(23) Petritsch, K.; Dittmer, J. J.; Marseglia, E. A.; Friend, R. H.; Lux, A.; Rozenberg, G. G.; Moratti, S. C.; Holmes, A. B. *Sol. Energy Mater. Sol. Cells* **2000**, *61*, 63.
(24) Benten, H.; Kudo, N.; Ohkita, H.; Ito, S. *Thin Solid Films* **2009**, *517*, 2016.
(25) Ma, C.-Q.; Mena-Osteritz, E.; Debaerdemaeker, T.; Wienk, M. M.; Janssen, R. A. J.; Bäuerle, P. *Angew. Chem., Int. Ed.* **2007**, *46*, 1679.
(26) Fischer, M. K. R.; Ma, C.-Q.; Janssen, R. A. J.; Debaerdemaeker, T.; Bäuerle, P. *J. Mater. Chem.* **2009**, DOI: 10.1039/b904243a.

Scheme 1. Synthesis of RuPcCOPy-*n*T and RuPc(Py-*n*T)$_2$ Series

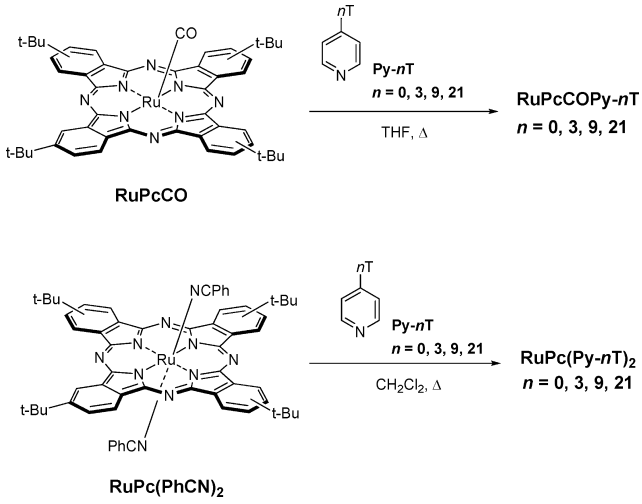

phthalocyanine dendritic oligothiophene complexes are depicted in Figure 1. Two different series of these hybrid molecules have been synthesized. The first series contains one Py-*n*T and one carbon monoxide as axial ligands (RuPcCOPy-*n*T), and the other series contains two axial Py-*n*T ligands (RuPc(Py-nT)$_2$).

In this paper we report about the synthesis of these complexes together with the extensive investigation on their optical and electrochemical properties and their application in BHJSCs.

Results and Discussion

Synthesis. The preparation of the RuPcCOPy-*n*T or RuPc(Py-*n*T)$_2$ complexes (n = 0, 3, 9, 21) bearing one or two Py-*n*T ligands at the axial positions of the RuPc is outlined in Scheme 1. Thus, pyridine-functionalized dendritic oligothiophenes Py-*n*T[26] of different generations (G1 n = 3, G2 n = 9 and G3 n = 21) were reacted with RuPcCO or RuPc(PhCN)$_2$ in refluxing THF or dichloromethane, respectively, yielding the corresponding hybrid systems as a result of the displacement of the labile ligands by Py-*n*Ts. In the case of the carbonyl derivative RuPcCO, the stronger CO−Ru bond prevents the exchange of the CO-ligand which is still present in the final products (RuPcCOPy-*n*T) incorporating only one dendritic Py-*n*T ligand. Reference complexes (RuPc(Py)$_2$ and RuPcCOPy) without thiophenes (n = 0) have also been prepared to evaluate the influence of the new pyridine functionalized DOT ligands.

All the RuPc dendritic oligothiophene complexes exhibit good solubility in common organic solvents and enough stability toward silica gel allowing an easy purification of these molecules by column chromatography and standard characterization by ^{1}H NMR, IR, UV/vis spectroscopy and MS spectrometry.

The absence of any important aggregation phenomena in solution allowed the characterization of these hybrid Pc-DOT molecules by ^{1}H NMR spectroscopy. The spectra of the RuPcCOPy-*n*T and RuPc(Py-*n*T)$_2$ complexes in $CDCl_3$ (see Supporting Information) show very nice resolved sets of signals attributed to the phthalocyanine ring protons at 9.4, 9.3, and 8.2 ppm and the diagnostic doublets at 5.3 and 2.0 ppm for 4-substituted pyridine ligands coordinated at the axial positions of the RuPc, considerably upfield shifted due to the strong ring current of the macrocycle. NMR dilution experiments were performed in the range of 10^{-3} to 10^{-4} M concentrations for the larger complex RuPc(Py-21T)$_2$, which showed no significant changes in the chemical shifts of the resonances assigned to the Pc ring. Indeed, the orthogonal arrangement of Pc and DOT units completely prevents the $\pi-\pi$ interaction between adjacent macrocycles. In contrast, protons corresponding to the axial ligands (both thiophene and pyridine units) proved to be slightly more sensitive toward concentration, indicating a small degree of aggregation of the molecules at this range of concentrations through the DOT axial ligands. On the other hand, our DOTs ligands are not flat but spherical molecules, and therefore $\pi-\pi$ stacking is substantially reduced in comparison with other dendritic oligothiophenes.

Additionally, the thermal stability of all complexes (except RuPc(Py)$_2$ and RuPcCOPy) was verified in the relevant temperature range for solar cells by means of differential scanning calorimetry (DSC). Indeed, no decomposition, melting or liquid crystalline behavior was observed between 50 and 250 °C.

Optical Properties. The absorption spectra of RuPcCOPy-*n*T and RuPc(Py-*n*T)$_2$ (Figure 2, Table 1) are dominated by intense Q- (i.e., 630 and 650 nm) and Soret-bands (i.e., 300−325 nm region) of the RuPc.[27−30] Notable is a significant broadening of the Q-band features, when two Py-*n*T ligands are attached to RuPc (Figure 2 right).

Besides these bands, additional absorption maxima can be found in the region between 350 and 550 nm. The intensity increases in this region and the general position redshifts with increasing generation of the Py-*n*T ligands. The absorption over this broad range stems from $\pi-\pi$*-transitions within the Py-*n*T ligands.

No significant changes in the absorption profile of the complexes were observed for different concentrations (between 1×10^{-7} and 1×10^{-3} M), confirming that no crucial aggregation in solution is occurring.

Electrochemical Properties. The HOMO/LUMO energy levels and corresponding band gaps of all complexes were determined by cyclic voltammetry (CV) in combination with differential pulse voltammetry (DPV) in CH_2Cl_2 solution. Data are collected in Table 2, and selected cyclic voltammograms are shown in Figures 3 and 4.

The E^0_{red1} and E^0_{ox1} potentials are attributed to a one-electron reduction ($Pc^{2-}Ru^{II}/Pc^{3-}Ru^{II}$) and a one-electron oxidation ($Pc^{2-}Ru^{II}/Pc^{-}Ru^{II}$) of the Pc macrocycle, respectively. In general, since the CO ligand is a strong π-acceptor, the reduction of the macrocycle in the RuPcCOPy-*n*T complexes is facilitated (−1.60 V compared to first reduction potentials at around −1.90 V in the case of the RuPc(Py-*n*T)$_2$ complexes).[31,32]

The values also indicate an influence of the dendritic oligothiophene at the pyridine on the redox processes of the Pc macrocycle. Although the electron-donating ability does slightly increase for the Py-*n*T ligands with increasing generation, this trend is not completely transferred to the E^0_{ox1} potentials of the hybrids. In the RuPcCOPy-*n*T family an easier first oxidation can only be observed for RuPcCOPy-3T when compared to the reference RuPcCOPy without thiophenes. For RuPcCOPy-9T and RuPcCOPy-21T, on the other hand, the first oxidation waves were observed at more positive values. The oxidation processes

(27) Bulatov, A.; Knecht, S.; Subramanian, L. R.; Hanack, M. *Chem. Ber.* **1993**, *126*, 2565.
(28) Bressan, M.; Celli, N.; d'Alessandro, N.; Liberatore, L.; Morvillo, A.; Tonucci, L. *J. Organomet. Chem.* **2000**, *593−594*, 416.
(29) Alagna, L.; Capobianchi, A.; Casaletto, M. P.; Mattogno, G.; Paoletti, A. M.; Pennesi, G.; Rossi, G. *J. Mater. Chem.* **2001**, *11*, 1928.
(30) Gorbunova, Y. G.; Enakieva, Y. Y.; Sakharov, S. G.; Tsivadze, A. Y. *Russ. Chem. Bull.* **2004**, *53*, 74.
(31) Rawling, T.; McDonagh, A. *Coord. Chem. Rev.* **2007**, *251*, 1128.
(32) Weidemann, M.; Hückstädt, H.; Homborg, H. *Z. Anorg. Allg. Chem.* **1998**, *624*, 846.

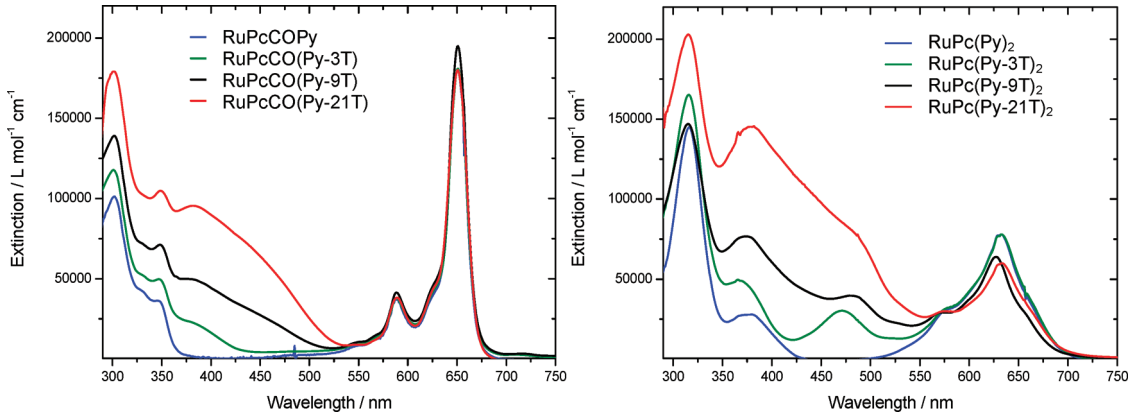

Figure 2. UV−vis spectra of RuPcCO(Py-*n*T) (left) and RuPc(Py-*n*T)$_2$ (right) in $CHCl_3$ ($c \approx 10^{-5}$ mol/L).

Table 1. Optical Absorption of RuPcCO(Py-*n*T) and RuPc(Py-*n*T)$_2$ Complexes in Comparison with Py-*n*T Ligands[a]

	absorption[b]			
compound	λ_1 (nm)	λ_2 (nm)	λ_3 (nm)	λ_4 (nm)
RuPcCO(Py-3T)	301	348	588	651
RuPc(Py-3T)$_2$	316	366	472	633
RuPcCO(Py-9T)	301	348	588	651
RuPc(Py-9T)$_2$	315	373	480	630
RuPcCO(Py-21T)[c]	301	348	588	651
RuPc(Py-21T)$_2$	315	379	480	633

[a] Extinction coefficients for the absorption are given in the experimental part. [b] In chloroform ($c \approx 1 \times 10^{-5}$ mol/L). [c] Additional maximum at $\lambda = 382$ nm.

Table 2. Electrochemical Properties of Hybrids RuPcCO(Py-*n*T) and RuPc(Py-*n*T)$_2$ in Comparison with RuPcCOPy, RuPc(Py)$_2$ and Py-*n*T References[26]

compound	E^0_{red1} (V):[a,b] Pc^{2-}/Pc^{3-}	E^0_{ox1} (V):[a,b] Pc^{2-}/Pc^{-}	E^0_{ox2} (V)[a,b]	HOMO (eV)[d]	LUMO (eV)[d]
Py-3T			0.91	−5.90	−2.96[e]
Py-9T			0.61	−5.61	−3.20[e]
Py-21T			0.41[c]	−5.47	−3.34[e]
RuPcCOPy	−1.69	0.09	0.88	−5.12	−3.57
RuPcCO(Py-3T)	−1.69	0.04	0.79	−5.13	−3.58
RuPcCO(Py-9T)	−1.58	0.25	0.62	−5.29	−3.60
RuPcCO(Py-21T)	−1.55	0.31		−5.31	−3.66
RuPc(Py)$_2$	−1.86	0.11	0.82	−5.15	−3.82
RuPc(Py-3T)$_2$	−1.86	0.11	0.81	−5.10	−3.71
RuPc(Py-9T)$_2$	−1.89	0.11	0.68	−5.10	−3.67
RuPc(Py-21T)$_2$	−1.90	0.12		−5.01	−3.59

[a] Measured in CH_2Cl_2/$TBAPF_6$ (0.1 M), $c = 1.0 \times 10^{-3}$ mol L^{-1}, 295 K, $v = 100$ mV s^{-1} vs Fc^+/Fc. [b] Values determined by DPV measurement. [c] Determined at $I^0 = 0.855I$.[47] [d] Calculated from E^{onset}_{red1} and E^{onset}_{ox1} set $E_{HOMO}(Fc^+/Fc) = -5.1$ eV.[48] [e] Measured in DMF/$TBAPF_6$ (0.1M), $c = 1.0 \times 10^{-3}$ mol L^{-1}, 295 K, $v = 100$ mV s^{-1} vs Fc^+/Fc.

are, except for RuPcCOPy, not reversible due to free α-positions at the thiophene rings in the periphery of the Py-*n*T ligands which dimerize upon oxidation.[33] The reduction of the phthalocyanine is easier the higher the generation of the Py-*n*T ligand and hence follows the same trend as the oxidation. The LUMO levels for the RuPcCO(Py-*n*T) series were measured to be approximately at −3.6 eV and do not change significantly for the different generations. In a similar way, the HOMO levels differ only by maximal 0.19 eV.

For the RuPc(Py-*n*T)$_2$ complexes the first one-electron oxidation process is observed at 0.11 V and the first reduction at approximately −1.8 V for all generations of the ligands and correspond to literature values for similar systems (Figure 3).[34] Hence, the HOMO levels are all similar in this series and located at approximately −5.1 eV. The LUMO levels follow the same trend and increase in energy from −3.82 eV for RuPc(Py)$_2$ to −3.59 eV for RuPc(Py-21T)$_2$. The most remarkable differences were observed for the second reduction processes that were found at −2.15 V for RuPc(Py-3T)$_2$ and at −2.06 V for RuPc(Py-9T)$_2$. These values match with the reduction potentials of the free Py-*n*T ligands.

Bulk Heterojunction Solar Cells. As the absorption of the PcRu hybrids was broadened by the attachment of the Py-*n*T ligands to the Pc and also the LUMO energy levels were determined to be high enough in energy for an efficient electron transfer to PCBM-derivatives, the nicely soluble complexes were used in solution processed bulk heterojunction solar cells (BHJSC). The devices were of the structure glass/ITO/PEDOT:PSS/$PC_{61/71}BM$ + RuPcCO$_x$(Py-*n*T)$_{2-x}$ /LiF/Al. The PEDOT:PSS layer was spin-cast from aqueous solution and $PC_{61/71}BM$ together with the RuPc-complex from chlorobenzene. LiF and aluminum were vacuum-deposited. The RuPc-complexes were mixed with $PC_{61}BM$ in ratios of 1:1, 1:2, 1:3 and 1:4. For all complexes the most effective cells were obtained at a 1:2 ratio. Some devices were prepared using $PC_{71}BM$ as acceptor at a ratio of 1:2. Also, different active layer thicknesses were made by adjusting the speed of the spin-casting process. A speed of 1000 rotations per minute afforded the best devices in almost all cases. This procedure gave active layers with thicknesses of 56−87 nm. The morphology of the active layer in bulk heterojunction solar cells is important for the performance of the devices.[35−38] The interpenetrating network of the active layer expands the photogeneration region of the device in comparison to a bilayer structure allowing more excitons to dissociate into free charge carriers. We investigated the morphology of the optimized devices (without the aluminum counter electrode) of RuPcCOPy-3T and RuPcCOPy-9T by atomic force microscopy (AFM) in tapping-mode. We chose these two compounds as

(33) You, C.-C.; Espindola, P.; Hippius, C.; Heinze, J.; Würthner, F. *Adv. Funct. Mater.* **2007**, *17*, 3764.
(34) Rawling, T.; Xiao, H.; Lee, S. T.; Colbran, S. B.; McDonagh, A. M. *Inorg. Chem.* **2007**, *46*, 2805.
(35) van Duren, J. K. J.; Yang, X.; Loos, J.; Bulle-Lieuwma, C. W. T.; Sieval, A. B.; Hummelen, J. C.; Janssen, R. A. J. *Adv. Funct. Mater.* **2004**, *14*, 425.
(36) Hoppe, H.; Niggemann, M.; Winder, C.; Kraut, J.; Hiesgen, R.; Hinsch, A.; Meissner, D.; Sariciftci, N. S. *Adv. Funct. Mater.* **2004**, *14*, 1005.
(37) Hoppe, H.; Sariciftci, N. S. *J. Mater. Chem.* **2006**, *16*, 45.
(38) Campoy-Quiles, M.; Ferenczi, T.; Agostinelli, T.; Etchegoin, P. G.; Kim, Y.; Anthopoulos, T. D.; Stavrinou, P. N.; Bradley, D. D. C.; Nelson, J. *Nat. Mater.* **2008**, *7*, 158.

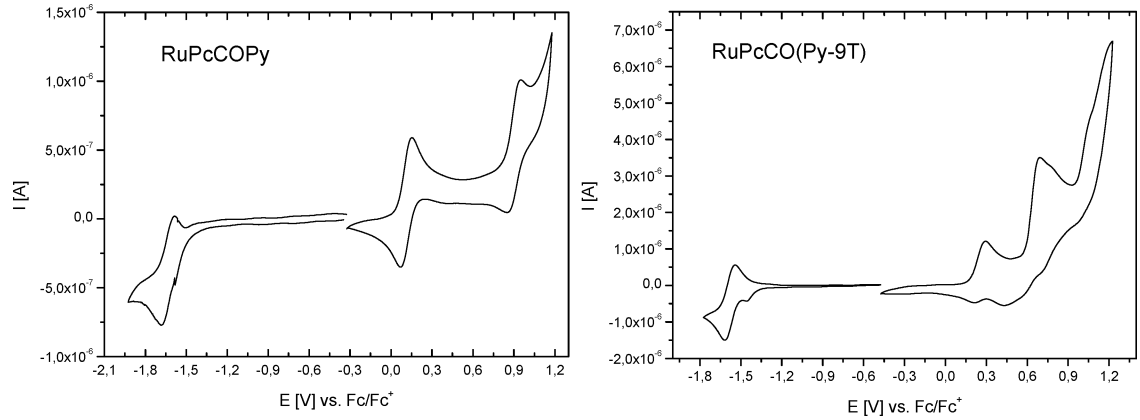

Figure 3. Cyclovoltammograms of RuPcCOPy (left) as reference and RuPcCO(Py-9T) exemplary for the RuPcCO(Py-*n*T) series.

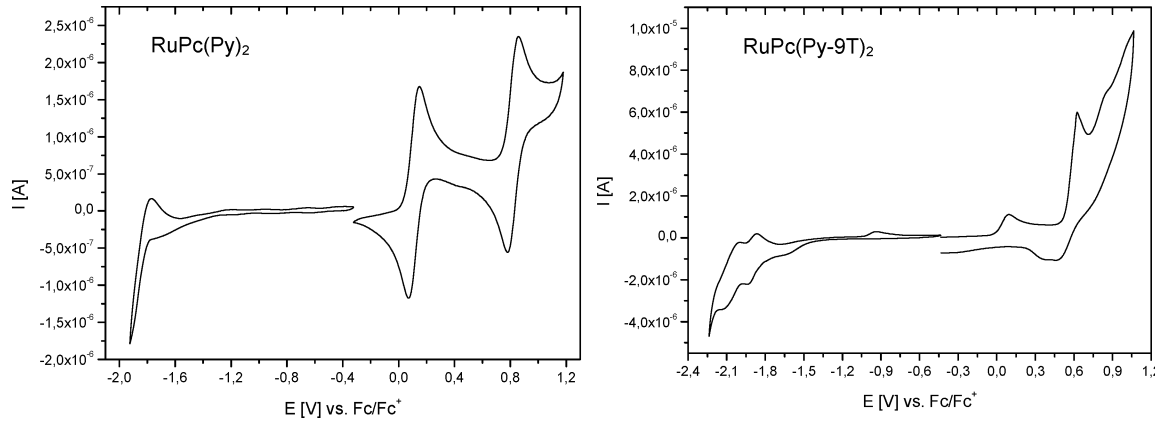

Figure 4. Cyclovoltammograms of $RuPc(Py)_2$ (left) as reference and $RuPc(Py\text{-}9T)_2$ exemplary for the $RuPc(Py\text{-}nT)_2$ series.

RuPcCOPy-3T showed good efficiencies of 1.0% whereas RuPcCOPy-9T showed bad efficiencies of only 0.4% in the solar cells. Figures S1 and S2 in the Supporting Information show relatively smooth films in the topography image without distinct features for both compounds, thus indicating that no phase separation on a larger scale (demixing) is present so that the formation of larger PCBM aggregates can be excluded.[39,40] The contrast observed in the nanometer scale of the phase images (more pronounced in the case of RuPcCOPy-9T) represents areas of different material composition.[41−43]

The solar cell results are summarized in Table 3.

For the RuPc bearing two pyridine-functionalized dendritic oligothiophenes in the axial positions with $PC_{61}BM$ as acceptor the short circuit current densities (J_{SC}) are generally high, varying between 2.8 and 5.1 mA cm^{-2}. The FFs range around 0.35 for all devices and are therefore one of the limiting factors for the cell performance. The open circuit voltage (V_{OC}) systematically increases with increasing size of the Py-*n*T ligands. The origin of this effect is not clear, because all PcRu hybrids have similar oxidation potentials suggesting invariable HOMO levels. The best efficiencies of 1.0% were accomplished with complex $RuPc(Py\text{-}3T)_2$ and $RuPc(Py\text{-}9T)_2$. The reference complex $RuPc(Py)_2$, without thiophene units in the axial ligands, showed the lowest efficiency of 0.6% due to the low V_{OC} of 0.44 V and the lowest FF of 0.28. For all complexes EQE-maxima are observed at around 630 or 660 nm, where the maximum of the Q-band absorption of the Pc macrocycle is located, indicating that predominantly the phthalocyanine is contributing to the photocurrent (Figure 5). These spectral response measurements suggest that the Py-*n*T ligands have two counteracting effects on the solar cell performance. On one hand the ligands increase the absorption, as can be seen from the higher EQE values in the area between 300 and 500 nm, but

Table 3. Characteristic Solar Cell Data

donor	thickness (nm)[b]	V_{OC} (V)	FF	J_{SC} (mA cm^{-2})[c]	η (%)
RuPcCOPy	73	0.63	0.31	4.6	0.9
RuPcCO(Py-3T)	65	0.60	0.37	4.5	1.0
RuPcCO(Py-9T)	65	0.34	0.27	3.9	0.4
RuPcCO(Py-21T)	56	0.48	0.35	4.1	0.7
$RuPc(Py)_2$	81	0.44	0.28	4.4	0.6
$RuPc(Py\text{-}3T)_2$	56	0.55	0.37	5.1	1.0
$RuPc(Py\text{-}9T)_2$	67	0.64	0.34	4.4	1.0
$RuPc(Py\text{-}21T)_2$	63	0.73	0.33	2.8	0.7
$RuPc(Py\text{-}3T)_2$[a]	67	0.55	0.38	7.1	1.5
RuPcCO(Py-3T)[a]	87	0.56	0.34	8.3	1.6

[a] Solar cells have been prepared with a spin coating speed of 1000 rpm and a donor−PCBM ratio of 1:2 except the cell of $RuPc(Py\text{-}21T)_2$ with a rotation speed of 750 rpm; $PC_{71}BM$ as acceptor. [b] Thickness of donor/PCBM layer. [c] From convolution of the EQE with AM1.5G.

(39) Troshin, P. A.; Hoppe, H.; Renz, J.; Egginger, M.; Mayorova, J. Y.; Goryachev, A. E.; Peregudov, A. S.; Lyubovskaya, R. N.; Gobsch, G.; Sariciftci, N. S.; Razumov, V. F. *Adv. Funct. Mater.* **2009**, *19*, 779.
(40) Zoombelt, A. P.; Gilot, J.; Wienk, M. M.; Janssen, R. A. J. *Chem. Mater.* DOI: 10.1021/cm900184z.
(41) Godehardt, R.; Lebek, W.; Adhikari, R.; Rosenthal, M.; Martin, C.; Frangov, S.; Michler, G. H. *Eur. Polym. J.* **2004**, *40*, 917.
(42) Salmerón Sánchez, M.; Molina Mateo, J.; Romero Colomer, F. J.; Gómez Ribelles, J. L. *Eur. Polym. J.* **2006**, *42*, 1378.
(43) Eaton, P.; Estarlich, F. F.; Ewen, R. J.; Nevell, T. G.; Smith, J. R.; Tsibouklis, J. *Langmuir* **2002**, *18*, 10011.

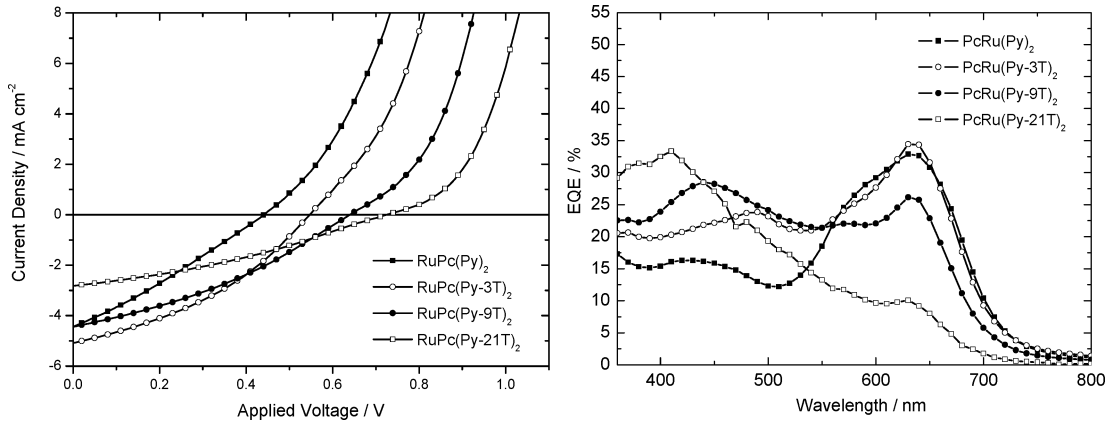

Figure 5. $J-V$ curves of the solar cells of the RuPc(Py-nT)$_2$ series (left) and corresponding EQE spectra of the devices (right).

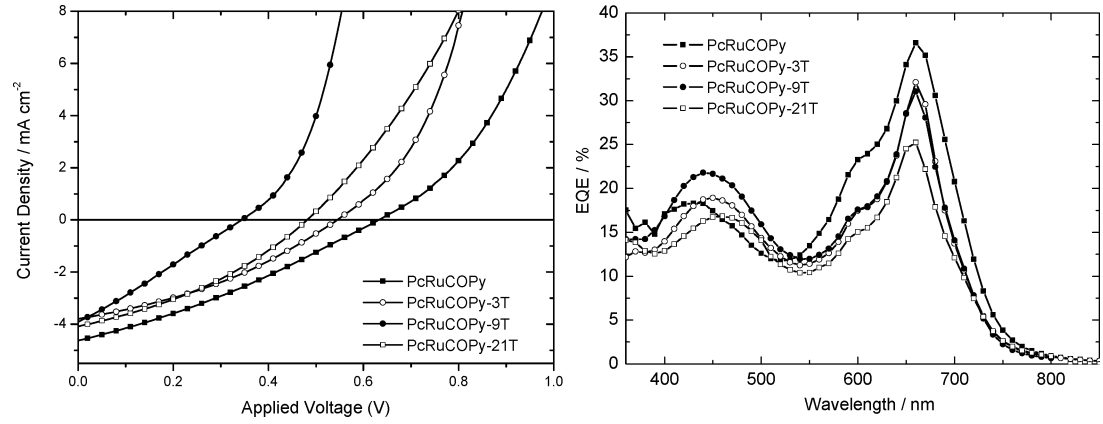

Figure 6. $J-V$ curves of the solar cells prepared from the RuPcCOPy-nT complexes (left) and corresponding EQE spectra of the devices (right).

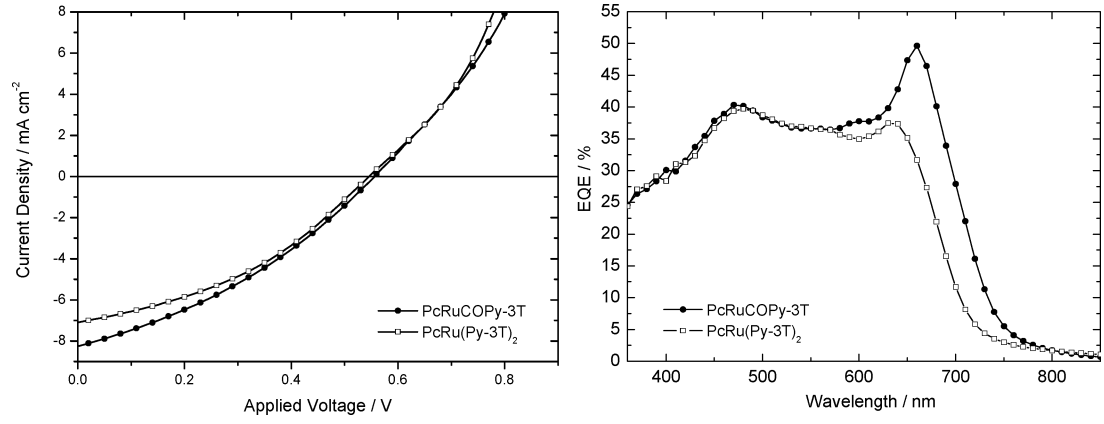

Figure 7. $J-V$ curves of the solar cells prepared from RuPcCO(Py-3T) and RuPc(Py-nT)$_2$ (left) and corresponding EQE spectra of the devices (right).

on the other hand, the Py-nT ligands seem to hamper the contribution of the macrocycle to the solar cell performance. The EQE values around 630 nm for RuPc(Py-nT)$_2$ and 660 nm for RuPcCO(Py-nT), respectively, are highest for the reference complexes without thiophenes and decrease with increasing generation of the axial ligands. This effect is more pronounced for the complexes with two Py-nT ligands but can also be observed for the other complex series. This could be due to steric hindrance, hampering either charge generation or charge collection. The complexes with the Py-3T ligands seem to have the best balanced relation between these two effects. Here the charge generation from the macrocycle is not yet too much hampered to annihilate the enhanced charge generation in the short wavelength area.

The current density−voltage curves ($J-V$ curves) of the solar cells from the RuPcCO(Py-nT) series are presented in Figure 6. For this series efficiencies were comparable to those of the symmetric donor molecules. The cell engineered from the first generation complex RuPcCO(Py-3T) gave the best efficiency of 1.0%. For the asymmetric donor molecules the trend of the V_{OC} with changing ligand size is less clear, but it seems to decrease with increasing size. This is actually opposite of what one would expect based on the decreasing HOMO levels for larger Py-nT ligands in the complexes.

From both series the most efficient complexes were tested in devices with $PC_{71}BM$ as acceptor, to further increase light absorption in the photo active layer (Figure 7).[44] The V_{OC} and FF for these cells are comparable to the cells using $PC_{61}BM$, but due to the $PC_{71}BM$ absorption, the current density significantly increases. The contribution of the $PC_{71}BM$ to the spectral response can most clearly be seen between 450 and 550 nm, but the EQE values increase over the entire spectral range. Consequently, for RuPcCO(Pyr-3T) the efficiency increases about 60% and for $RuPc(Py\text{-}3T)_2$ about 40%. These devices reach a J_{SC} of up to 8.3 mA cm^{-2} (RuPcCOPy-3T), which is particularly high for solution processed small molecule bulk heterojunction solar cells.

Hence, the new soluble phthalocyanine complexes were applied successfully in solution processed BHJSCs. For the first time the efficiencies of the solution processed phthalocyanine-based solar cells are comparable to those of the vacuum deposited ones.

Conclusion

We presented two series of highly soluble RuPc complexes with pyridine functionalized dendritic oligothiophenes as axial ligands. With the help of the ligands it was possible to enhance the absorption between 380 and 550 nm where RuPcs do not exhibit a strong absorption and to improve therefore the light-harvesting ability. Electrochemical structure−property relations of the complexes could be derived by cyclovoltammetry. The applicability of the complexes for BHJSCs could be ensured due to gained HOMO/LUMO energy levels, whereas it was difficult to correlate the characteristic solar cell data, especially the open circuit voltage, with the energy levels. Furthermore we fabricated solution processed bulk heterojunction solar cells of all compounds with high efficiencies of up to 1.6%. For the first time the efficiencies of the solution processed phthalocyanine-based solar cells are comparable to those of the vacuum deposited ones. By analysis of the solar cell data we were able to derive relations between the structure, especially the generation of the dendritic ligand, and the solar cell performance.

Experimental Section

General Procedures. NMR spectra were recorded on a Bruker AC-300 instrument at 25 °C. Thin layer chromatography was carried out on aluminum plates, precoated with silica gel, Merck Si60 F_{254}. Preparative column chromatography was performed on glass columns packed with silica gel, Merck silica 60 (230−400 mesh, 60 Å). BIO BEADS S-X1 beads (200−400 mesh) were purchased from BIO-RAD LABORATORIES. EI mass spectra were recorded with a hybrid QTOF analyzer MODEL QSTAR pulsar I from Applied Biosystem. MALDI-TOF spectra on a Bruker Daltonics Reflex III using DCTB (*trans*-2-[3-(4-*tert*-butylphenyl)-2-methyl-2-propenylidene]malononitrile). We used a Mettler Toledo DSC823^e differential scanning calorimeter to check the thermal stability and solid state behavior. A Veeco diMultiMode V atomic force microscope was used to investigate the morphology of the active layers of the solar cell devices. Optical measurements were carried out in 1 cm cuvettes with Uvasol grade solvents, absorption spectra recorded on Perkin-Elmer Lambda 19 and Hewlett-Packard 8453 spectrophotometers. Cyclic voltammetry experiments were performed with a computer-controlled EG&G PAR 273 potentiostat in a three-electrode single-compartment cell with a platinum working electrode, a platinum wire counter electrode, and an Ag/AgCl reference electrode. All potentials were internally referenced to the ferrocene/ferrocenium couple.

Solar Cells. The photovoltaic devices were prepared by spin coating EL-grade PEDOT:PSS (Clevios P VPAI4083; H. C. Starck) onto cleaned, patterned indium tin oxide (ITO) substrates (14 Ω cm^{-2}). The photoactive layer was deposited by spin-coating from a chlorobenzene solution with a total concentration of 25 mg/mL. Film thicknesses were determined by profilometry (Veeco Dektak 150). The counter electrode of LiF (1 nm) and aluminum (100 nm) was deposited by vacuum evaporation at around 1×10^{-6} mbar. The active area of the cells was 0.167 cm^2. Spectral response was measured with a Keithley 2400 source meter, using monochromatic light from a tungsten halogen lamp in combination with monochromator (Oriel, Cornerstone 130). A calibrated Si cell was used as reference. The device was kept behind a quartz window in a nitrogen filled container. $J-V$ characteristics were measured under ca. 100 mW cm^{-2} simulated solar light from a tungsten−halogen lamp (Philips Brilliantline Pro) filtered by a Schott GG 385 and a Hoya LB 120 filter. The exact current density was calculated by convolution of the spectral response with the AM1.5G spectrum (100 mW cm^{-2}).

Synthesis. Tetra-*tert*-butylphthalocyanine and $Ru_3(CO)_{12}$ were purchased from Aldrich Chemical Co. and used as received without further purification. RuPcCO, RuPcCOPy, $RuPc(PhCN)_2$ and $RuPc(Py)_2$ were prepared following procedures described in the literature.[45,46]

Preparation of RuPcCOPy-nT (n = 3, 9, 21). A solution of RuPcCO (0.052 mmol) and Py-*n*T ligand (0.044 mmol) in THF (4 mL) was stirred under argon and heated at 40 °C for 2 h. The solvent was evaporated and the solid purified by column chromatography (CH_2Cl_2/hexane, 2:1). The green fraction was collected and the solvent removed yielding 80−85% of RuPcCOPy-*n*T as a dark green powder.

RuPcCO(Py-3T). ^{1}H NMR (300 MHz, $CDCl_3$): δ (ppm) = 9.4 (m, 4H, H^{Pc}), 9.3 (m, 4H, H^{Pc}), 8.1 (m, 4H, H^{Pc}), 7.1 (m, 2H), 6.7 (m, 3H), 6.65 (dd, J = 3.6, 1.1 Hz, 1H), 6.45 (s, 1H), 5.42 (d, J = 6.9 Hz, 2H, Py), 1.98 (d, J = 6.9 Hz, 2H, Py), 1.7 (m, 36H, $C(CH_3)_3$). UV/vis ($CHCl_3$): λ_{max} (nm) (ε, $\times 10^3$ M^{-1} cm^{-1}) = 301 (118), 347 (50), 588 (38), 651 nm (181). IR (KBr): ν (cm^{-1}) = 3082, 2960, 2905, 2869, 1976 (CO), 1612, 1492, 1394, 1386, 1323, 1317, 1257, 1155, 1126, 1093, 1051, 941, 831, 767, 696, 671. HR-ESI (methanol + 1% formic acid) calcd for $C_{66}H_{60}N_9OS_3Ru$, $[M + H]^+$, m/z: 1192.3137; found 1192.3077.

RuPcCO(Py-9T). ^{1}H NMR (300 MHz, $CDCl_3$): δ (ppm) = 9.4 (m, 4H, H^{Pc}), 9.3 (m, 4H, H^{Pc}), 8.1 (m, 4H, H^{Pc}), 7.2 (m, 4H), 6.9 (m, 12H), 6.74 (d, J = 3.8 Hz, 1H), 6.64 (d, J = 3.8 Hz, 1H), 6.45 (s, 1H), 5.41 (d, J = 6.9 Hz, 2H, Py), 1.99 (d, J = 6.9 Hz, 2H, Py), 1.7 (m, 36H, $C(CH_3)_3$). UV/vis ($CHCl_3$): λ_{max} (nm) (ε, $\times 10^3$ M^{-1} cm^{-1}) = 301 (139), 348 (71), 588 (41), 651 nm (195). IR (KBr): ν (cm^{-1}) = 3076, 2952, 2910, 2870, 1973 (CO), 1603, 1492, 1396, 1315, 1155, 1128, 1088, 1049, 939, 835, 768, 702. HR-ESI (methanol + 1% formic acid) calcd for $C_{90}H_{72}N_9ORuS_9$, $[M + H]^+$, m/z: 1684.2403; found 1684.2203.

RuPcCO(Py-21T). ^{1}H NMR (300 MHz, $CDCl_3$): δ (ppm) = 9.4 (m, 4H, H^{Pc}), 9.3 (m, 4H, H^{Pc}), 8.1 (m, 4H, H^{Pc}), 7.2 (m, 8H), 6.9 (m, 31H), 6.76 (d, J = 3.8 Hz, 1H), 6.67 (d, J = 3.8 Hz, 1H), 6.59 (d, J = 3.8 Hz, 1H), 6.38 (s, 1H), 5.31 (d, J = 6.9 Hz, 2H, Py), 1.98 (d, J = 6.9 Hz, 2H, Py), 1.7 (m, 36H, $C(CH_3)_3$). UV/vis ($CHCl_3$): λ_{max} (nm) (ε, $\times 10^3$ M^{-1} cm^{-1}) = 301 (179), 348 (105), 588 (38), 651 nm (180). IR (KBr): ν (cm^{-1}) = 3082, 2954, 2912, 2858, 1971 (CO), 1601, 1485, 1391, 1313, 1331, 1250, 1155, 1128,

(44) Wienk, M. M.; Kroon, J. M.; Verhees, W. J. H.; Knol, J.; Hummelen, J. C.; van Hal, P. A.; Janssen, R. A. J. *Angew. Chem., Int. Ed.* **2003**, *42*, 3371.

(45) Rodriguez-Morgade, M. S.; Torres, T.; Atienza-Castellanos, C.; Guldi, D. M. *J. Am. Chem. Soc.* **2006**, *128*, 15145.

(46) Rodriguez-Morgade, M. S.; Planells, M.; Torres, T.; Ballester, P.; Palomares, E. *J. Mater. Chem.* **2008**, *18*, 176.

(47) Adams, N. R. *Electrochemistry at Solid Electrodes*; M. Dekker: New York, 1969.

(48) Johansson, T.; Mammo, W.; Svensson, M.; Andersson, M. R.; Inganas, O. *J. Mater. Chem.* **2003**, *13*, 1316.

1088, 1049, 943, 833, 793, 690. HRMS (MALDI-TOF, DCTB) calcd for $C_{137}H_{95}N_9RuS_{21}$, $[M - CO]^+$, *m/z*: 2642.0904; found 2642.0928.

Preparation of RuPc(Py-nT)$_2$ (n = 3, 9, 21). A solution of $RuPc(PhCN)_2$ (0.050 mmol) and Py-*n*T ligand (0.15 mmol) in CH_2Cl_2 (5 mL) was stirred under argon and heated at reflux for 3 h. The solvent was evaporated and the solid purified by column chromatography (CH_2Cl_2/hexane, 2:1). The green fraction was collected and the solvent removed yielding 75% of RuPc(Py-*n*T)$_2$ (n = 3, 9) as a dark green powder. In the case of RuPc(Py-21T)$_2$ further purification was required by gel permeation chromatography (BIO BEADS S-X1 beads, THF) yielding 65% of a green solid.

RuPc(Py-3T)$_2$. ^{1}H NMR (300 MHz, $CDCl_3$): δ (ppm) = 9.2 (m, 4H, H^{Pc}), 9.1 (m, 4H, H^{Pc}), 7.9 (m, 4H, H^{Pc}), 7.1 (m, 4H), 6.7 (m, 6H), 6.65 (dd, J = 3.6, 1.1 Hz, 2H), 6.47 (s, 2H), 5.33 (d, J = 6.9 Hz, 4H, Py), 2.45 (d, J = 6.9 Hz, 4H, Py), 1.7 (m, 36H, $C(CH_3)_3$). UV/vis ($CHCl_3$): λ_{max} (nm) (ε, $\times 10^3$ M^{-1} cm^{-1}) = 316 (165), 366 (50), 472 (30), 633 nm (78). IR (KBr): ν (cm^{-1}) = 3084, 2953, 2912, 2872, 1603, 1491, 1396, 1319, 1294, 1254, 1148, 1094, 1053, 825, 764, 700. HR-ESI (methanol + 1% formic acid) calcd for $C_{82}H_{71}N_{10}RuS_6$, $[M + H]^+$, *m/z*: 1489.3225; found 1489.3244.

RuPc(Py-9T)$_2$. ^{1}H NMR (300 MHz, $CDCl_3$): δ (ppm) = 9.2 (m, 4H, H^{Pc}), 9.1 (m, 4H, H^{Pc}), 7.9 (m, 4H, H^{Pc}), 7.2 (m, 8H), 6.9 (m, 24H), 6.76 (d, J = 3.8 Hz, 2H), 6.65 (d, J = 3.8 Hz, 2H), 6.47 (s, 2H), 5.34 (d, J = 6.9 Hz, 4H, Py), 2.45 (d, J = 6.9 Hz, 4H, Py), 1.7 (m, 36H, $C(CH_3)_3$). UV/vis ($CHCl_3$): λ_{max} (nm) (ε, $\times 10^3$ M^{-1} cm^{-1}) = 316 (147), 373 (77), 480 (40), 633 nm (59). IR (KBr): ν (cm^{-1}) = 3065, 2953, 2939, 2858, 1610, 1487, 1393, 1366, 1312, 1285, 1258, 1217, 1149, 1122, 1082, 941, 827, 800, 696. MS (MALDI-TOF, DCTB): *m/z* = 2469.3−2480.3 $[M]^+$.

RuPc(Py-21T)$_2$. ^{1}H NMR (300 MHz, $CDCl_3$): δ (ppm) = 9.2 (m, 4H, H^{Pc}), 9.1 (m, 4H, H^{Pc}), 7.9 (m, 4H, H^{Pc}), 7.2 (m, 16H), 6.9 (m, 64H), 6.69 (d, J = 3.8 Hz, 2H), 6.61 (d, J = 3.8 Hz, 2H), 6.41 (s, 2H), 5.24 (d, J = 6.9 Hz, 4H, Py), 2.46 (d, J = 6.9 Hz, 4H, Py), 1.7 (m, 36H, $C(CH_3)_3$). UV/vis ($CHCl_3$): λ_{max} (nm) (ε, $\times 10^3$ M^{-1} cm^{-1}) = 315 (203), 379 (145), 480 (sh), 633 nm (60). IR (KBr): ν (cm^{-1}) = 3437, 3065, 2953, 2939, 2858, 1610, 1487, 1393, 1312, 1258, 1217, 1149, 1129, 1082, 941, 827, 800, 696. MS (MALDI-TOF, DCTB): *m/z* = 4439.8−4449.8 $[M]^+$. Anal. Calcd for $C_{226}H_{142}N_{10}RuS_{42}$: C, 61.06; H, 3.22; N, 3.15. Found: C, 60.87; H, 3.54; N, 3.19%.

Acknowledgment. This work was supported by the German Science Foundation (DFG) in the frame of the Collaborative Research Center (SFB) 569. We also would like to thank the Fonds der Chemischen Industrie for financial support. Grants from the Ministerio de Ciencia y Tecnología (CTQ2008-00418/BQU, Consolider-Ingenio 2010 CSD2007-00010 Nanociencia Molecular, ESF-MEC MAT2006-28180-E, SOHYDS), Comunidad de Madrid MADRISOLAR, S-0505/PPQ/0225) and the European Union (SOLAR n-TYPE, MRTN CT-2006-035533) are gratefully acknowledged. The authors want to thank Dr. Elena Mena-Osteritz and Eva-Kathrin Schillinger for measuring AFM images.

Supporting Information Available: AFM images of the active layers of the optimized devices of RuPcCOPy-3T (Figure S1) and RuPcCOPy-9T (Figure S2) and the ^{1}H NMR (Figures S3−S8) and IR spectra (Figures S9−S14) of all novel compounds. This material is available free of charge via the Internet at http://pubs.acs.org.

JA901537D